

Article

Sensitivity of Radiative and Thermal Properties of Building Material in the Urban Atmosphere

Marcos Vinicius Bueno de Morais ^{1,2,*} , Viviana Vanesa Urbina Guerrero ³,
Edmilson Dias de Freitas ² , Edson R. Marciotto ⁴, Hugo Valdés ⁵ , Christian Correa ⁶ ,
Roberto Agredano ⁶  and Ismael Vera-Puerto ⁶ 

¹ Departamento de Obras Civiles, Facultad de Ciencias de la Ingeniería, Universidad Católica del Maule, Av. San Miguel 3605, Talca 3480112, Chile

² Instituto de Astronomia, Geofísica e Ciências Atmosféricas, Universidade de São Paulo, São Paulo 05508-090, Brazil; edmilson.freitas@iag.usp.br

³ Atmospheric Extreme Events Laboratory, Federal Technology University—Paraná, Av. Pioneiros 3131, Londrina 86036-370, Paraná, Brazil; viviana.urbina@gmail.com

⁴ Department of Physics, Federal University of Santa Catarina, Bairro da Trindade-Florianópolis, Santa Catarina 88040-900, Brazil; e.r.marciotto@gmail.com

⁵ Centro de Innovación en Ingeniería Aplicada, Departamento de Computación e Industrias, Universidad Católica del Maule 3605, Talca 3480112, Chile; hvaldes@ucm.cl

⁶ Centro de Innovación en Ingeniería Aplicada, Departamento de Obras Civiles, Universidad Católica del Maule 3605, Talca 3480112, Chile; clcorrea@ucm.cl (C.C.); ragredano@ucm.cl (R.A.); ivera@ucm.cl (I.V.-P.)

* Correspondence: bmarcos@ucm.cl; Tel.: +56-712-203-566

Received: 13 November 2019; Accepted: 28 November 2019; Published: 3 December 2019



Abstract: In the context of the impact of urbanization on climate change, this work aims to evaluate the sensitivity of the thermal and radiative properties of building surfaces in urban areas to the urban heat island intensity, a local scale meteorological phenomenon. For this, variations of albedo values, emissivity, thermal conductivity and heat capacity of roofs, streets and walls were simulated through an urban scheme coupled with the BRAMS mesoscale atmospheric model for the metropolitan area of São Paulo, considering two main urban types. The simulations show that, in general, looking for cold surface situations, the change of building material can contribute to a reduction of up to 3 °C for São Paulo. In addition, the role of orientation and the typological characteristics of constructions should be taken into account. In this sense, it is expected that this work guides civil engineers and builders to search for new materials in order to reduce the effects of urbanization on the local climate.

Keywords: radiative and thermal properties; urban climate; Urban Heat Island; sustainable construction

1. Introduction

In recent years, the process of urbanization can be considered as one of the most impressive phenomena in the history of our planet. In 1950, only 29.1% of the world's population lived in urban areas. In 2018, this number increased to 55%, with the highest rate of increase being in less developed regions [1]. The number of cities with more than 10 million inhabitants (megacities) and their population are also increasing. In 1950, there were only two megacities (New York and Tokyo). There are currently 19 worldwide, 13 of them in emerging countries [1].

With this accelerated population growth, an increase in the urbanized area is also observed which can cause changes in the local climate of a region, since the process of urbanization causes changes in roughness, surface thermal properties, decreased wind intensity and soil moisture [2]. These changes generate a temperature difference between the urban and surrounding rural regions. The temperature contrast between these two regions is called Urban Heat Island (UHI) [3]. The UHI is associated with

large urban centers and is named after the shape of temperature isotherms close to the surface, similar to the topographical contours of an island in the middle of the sea, where regions of lower temperature surround the city. UHI is more evident during the night period [4] and the thermal contrasts between cities and rural areas can be higher than 10 °C [5].

The development of a UHI is due to processes such as the change in land use, which modifies the energy budget of the atmosphere [6]. Human activities, such as industry and traffic, also generate energy that contributes to urban heating [7–11]. Generally, UHI formation occurs when winds of synoptic-scale are weak [12], resulting in the development of convective circulations in large urban centers. In this condition, the concentration of pollutants can be higher when compared to those observed over rural areas [13,14]. In the case of urban areas near to the sea or located in irregular terrain, in addition to the circulation associated with UHI, there is a strong influence of sea/land and valley/mountain breezes [4,13,15,16].

The measurement of the UHI intensity is defined by the temperature difference between urban and rural regions [17]. This difference is due to the different properties of each type of surface, such as the albedo and the anthropogenic heat released [18–21]. Because the UHI intensity is highly dependent on the dimensions of the cities, in some cases of small towns, UHI may be imperceptible [12], because of the rapid mixing of air over the city with the air of neighboring regions.

UHI intensity characteristics vary under different weather conditions. It is possible to observe that, during cloudless conditions and weak winds, the differences between the temperature of the city and neighborhoods intensify in the late period [22,23]. However, in the daytime period, the inverse phenomenon can occur, with negative intensities of the UHI [24,25]. This effect, named Urban Cool Island, may be related to the type of material used in the constructions [26–28], the amount of vegetation [29,30], and the number of water bodies present in the city [31]. For Melbourne (Australia), the UHI intensity varies from -3.16 °C– 6 °C [32]. For example, in Shenyang, China, in the winter period, a cold island is formed during the day, whose intensity can reach values of -3.8 °C, as a product of the attenuating effect of the aerosols present in the urban atmosphere over solar radiation [33].

Numerical studies involving technologies of adaptation and mitigation of UHI are already being carried out in different cities across the world. In Chicago, for example, results indicate that the use of green and cool roofs can be a method to make cities more resilient against UHI [34], also, to contribute in reducing heat stress in vulnerable urban communities [35]. Considering an arid region, such as the Phoenix metropolitan area (Arizona), the implementation of these roofing systems reduces the sensible heat fluxes by up to 150 W/m² during the daytime, lowering the atmospheric boundary layer height by approximately 700 m [36]. This contributes to an increase in the convective available potential energy over the rural area, and its reduction over the urban core, enhancing the probability of precipitation towards the suburb region of the city. On the other hand, Song et al. [37] showed that, for the state of California, hybrids roofs (combined biophysical properties of green and cool roofs) can lead to a further 1 – 2 °C reduction in 2 m temperature during summer.

The high-temperature rise caused by urbanization, associated with the possible effects of climate change [38], has a direct impact on people's health [39]. Besides influencing directly in the thermal comfort of the people [40], the increase of temperature also tends to increase the transmission of diseases in vulnerable countries [41,42]. In this way, aiming at the sustainable building to the urbanization process [43], researchers have been looking for new building materials in order to be energy efficient and sustainable in order to produce less atmospheric contamination and consequently decrease the intensity of UHI [44]. Also, these materials have sought to reduce the environmental impact of the building industry by including aggregate materials in the composition of structures [45]. In this sense, these materials seek to improve the physical, mechanical and thermal properties [46], often using recyclable materials [47,48].

Based on this, this work proposes to carry out a sensitivity study of the radiative and thermal properties of building materials in the urban microclimate, varying their magnitudes and verifying their impact on the variation of UHI intensity, using mesoscale atmospheric models. Also, an analysis

of these variables between the different urban types in the Metropolitan Area of São Paulo (MASP) is discussed [49]. It is hoped, therefore, to indicate a direction for construction engineers to pursue specific material standards in order to lessen the impact of urbanization on climate change.

2. Methodology

2.1. Study Area

The MASP is centered at $23^{\circ}52' S$ and $46^{\circ}70' W$ (Figure 1), about 60 km far from the Atlantic sea with a mean altitude of 775 m, with an area of 8051 km^2 [50]. Hot, humid summers characterize the urban area, with air temperatures varying between $22^{\circ} C$ and $30^{\circ} C$, and mild winters between $10^{\circ} C$ and $22^{\circ} C$. With more than 22 million inhabitants, MASP is considered a vulnerable area to climate change and local warming effects, driven by urbanization [51].

MASP is characterized by a heterogeneous urban structure (Figure 1), resulting from the rapid growth of the city during the 20th century [52]. The building typology is diverse within the urban area [53]. However, two typologies dominate [54]. Part of residential districts and the historical center are characterized by tower blocks (often above ten storeys) and a large number of high-rise buildings, herein called urban-type 1. In the peripheries of the urban area, buildings are typically one or two storeys, herein called urban-type 2. Based on Local Climate Zones (LCZ, [55]), the equivalence of these urban types would be LCZ 1 and 5 [14], respectively.

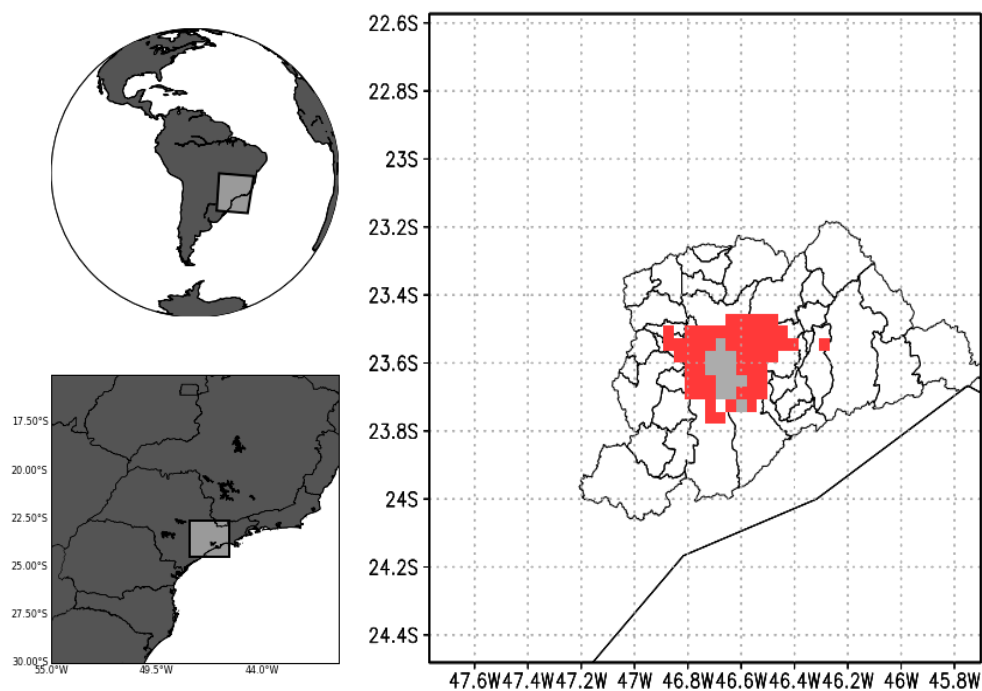


Figure 1. Localization of the Metropolitan Area of São Paulo (MASP). On the right map, the urban-type colors, where the gray color is the urban-type 1 and red color is the urban-type 2. The boundaries limits in the right map are the cities of MASP.

2.2. Numerical Modeling Description

To study the impact of different characteristics of building physical properties on the urban atmosphere, the Brazilian Developments on the Regional Atmospheric Modeling System (BRAMS, available at <http://brams.cptec.inpe.br/>) [56,57] was used. This mesoscale model is based on RAMS [58], and was originally modified to represent the atmospheric processes in tropical and sub-tropical regions. Figure 2 presents a model execution scheme. To run a simulation, it is necessary to execute three steps. In the preprocessing stage, a global circulation model output is used by the *geradp* program, which

formats the data to be an initial, boundary conditions, and nudging as input for the model. The *makesfc* program inserts the surfaces data (albedo, the vegetation fraction, topography, etc.) into the size of the selected grid. These data are usually obtained by remote sensing. To finalize the preprocessing stage, *makevfile* binds all the information from the other two programs and interpolates in the template grid. *BRAMS Initial* is the name of the kernel that represents the model execution. The post-processing step is given by the *RAMSPost* program, which extracts the desired variables (such as wind speed at 10 m, temperature and humidity at 2 m) in a format to be used in visualization software, such as GrADS, python or MATLAB.

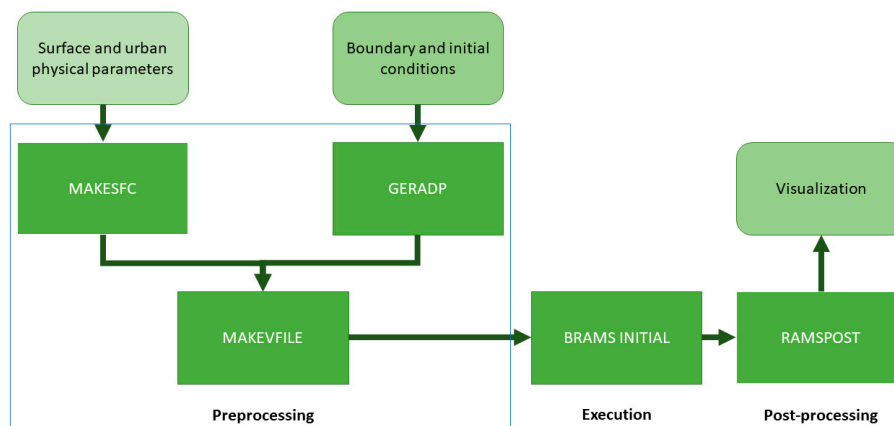


Figure 2. BRAMS' execution scheme.

The model can make use of multiple grid nesting schemes, that allows the solution of different meteorological phenomenon scales, since local to synoptic. It includes many physical parameterizations for land surface, boundary-layer, microphysics, convection and radiation processes. In this work, the 4.2 version of BRAMS 4.2 is used.

For surface-atmospheric interaction schemes, BRAMS includes the Land Ecosystem-Atmosphere Feedback (LEAF) [59] for vegetation, and Town Energy Budget (TEB) [60] for urban areas. This module represents the buildings as an urban canyon with infinite length, considering it has different three components: Walls, street and roof. With this configuration, the urban scheme allows solving energy budget equations for each surface. This scheme permits an appropriate representation for mesoscale analysis, of the turbulent heat fluxes to the urban atmosphere, as it accounts for most of the physical processes for the urban area [61]. The internal temperature of buildings (T_{ibld}) is independent of the external temperature [60] and the minimum value is assumed to be 22 °C [62]. The magnitude of T_{ibld} is calculated using a standard resistance equal to $0.123 \text{ K}\cdot\text{m}\cdot\text{W}^{-1}$ [61], based on building insulation values [63]. The TEB version used in this study also includes the effect of urban vegetation areas, by weighting the turbulent fluxes, as described in Morais et al. [26].

2.3. Simulations Descriptions

The simulations were executed considering a Control Simulation, which corresponds to the closest to the real, as validated in Morais et al. [26]. The model characteristics and physical parameterization are presented in Table 1, and for TEB, the main parameters are presented in Table 2. The values considered are the same as Freitas et al. [13]. The two main urban types within cities were considered in the classification methodology. Here, urban-type 1 represents a higher concentration of higher-rise buildings, while urban-type 2 represents small and medium-sized buildings (Figure 1). Following the limitations of the urban scheme in mesoscale modeling, the orientation of urban canyon for all simulation is assumed to be north-south [64]. The other simulations were done changing the magnitude of albedo, emissivity, thermal conductivity and heat capacity individually. The last two parameters are estimated in order to keep the same thermal admittance (μ) in $\text{J}\cdot\text{m}^{-2}\cdot\text{s}^{-1/2}\cdot\text{K}^{-1}$, as in Johnson et al. [65]:

$$\mu = (\lambda C)^{1/2}, \quad (1)$$

where λ is the thermal conductivity in $\text{W}\cdot\text{m}^{-1}\cdot\text{K}^{-1}$ and C , the heat capacity in $\text{J}\cdot\text{m}^{-3}\cdot\text{K}^{-1}$. These parameters represent the building material, and it was assumed for control simulation, considering an asphalt street, a mix of wood, concrete and brick wall, and a roof tile. These values are described on Freitas et al. [37], following the current Brazilian norms [66].

Table 1. Model's physical parameterizations and numerical options used in the experiments, following Morais et al. [26].

Physical	Options
Lateral boundary nudging points	5
Lateral boundary nudging time scale	3600 s
Top boundary nudging time scale	1800 s
Lateral Boundary Condition	Klemp [67]
Radiation parameterization	Chen & Cotton [68]
Radiation update timestep	3600 s
Soil layers depth	-2.0, -1.5, -0.25 and -0.05 m
Soil saturation degree	0.49, 0.44, 0.42, 0.35
Turbulence scheme	Smagorinski [69] modified by Hill [70] and Lilly [71]

Table 2. TEB parameters used in the experiments, following Freitas et al. [13].

Parameters	Urban 1	Urban 2
Roof Albedo	0.18	0.18
Street Albedo	0.08	0.08
Wall Albedo	0.14	0.14
Roof Emissivity	0.90	0.90
Street Emissivity	0.95	0.95
Wall Emissivity	0.90	0.90
Aspect-Ratio	10	0.6
Building Heights (m)	50	5
Roughness Length (m)	3	0.5
Traffic Sensible Heat Flux ($\text{W}\cdot\text{m}^{-2}$)	90	10
Traffic Latent Heat Flux ($\text{W}\cdot\text{m}^{-2}$)	10	5
Industrial Sensible Heat Flux ($\text{W}\cdot\text{m}^{-2}$)	14	10
Industrial Latent Heat Flux ($\text{W}\cdot\text{m}^{-2}$)	50	30

The analyses of the Global Forecasting System (GFS) with 1° of horizontal spacing grid, provided by the National Centers for Environmental Prediction (NCEP), were used as initial and boundary condition. The study period is from 00Z of 17 July 2008–00Z of 20 July 2008, which correspond to clear days, without cloud or rain, to get better results analysis about the urban effect. The first 24 h were discarded to remove the spin-up effect [72]. Figure 3 presents the two nested grids that were used in the simulations. The domain resolution was 16 km and 4 km. The topographical data was provided by the US Geological Survey, with 1 km of spatial grid spacing. NDVI product data with 250 m of resolution from the MODIS sensor for 18 July 2008 was used to obtain the vegetation fraction [73]. For all simulations, it was assumed short grass for both urban areas. This model was previously validated on Morais et al. [26], for the same period.

To consider the influence of urban area to the regional environment, the results analysis was done considering not only the UHI intensity and its comparison between both LCZs. To obtain the UHI, a simulation changing the urban area by the Mixed Forest was done, predominant land surface type around the MASP. The UHI magnitude was calculated by the difference between the simulations with and without urban area.

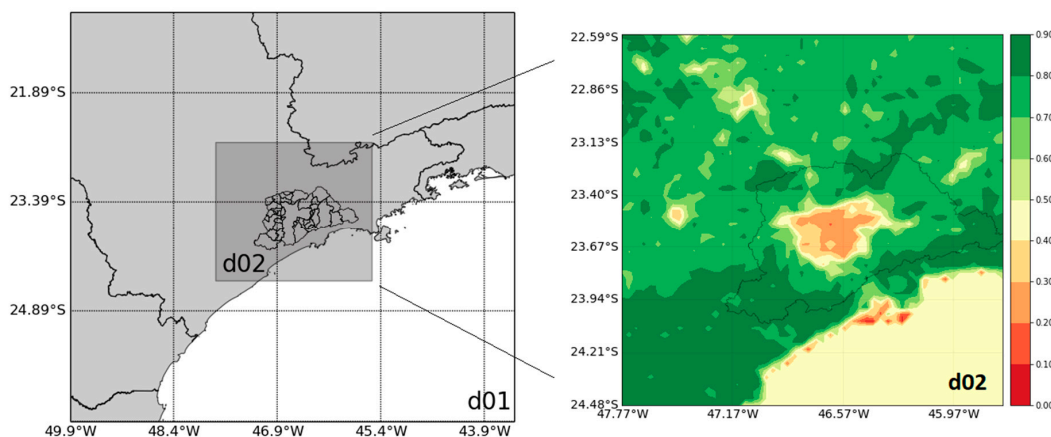


Figure 3. The two domains and NDVI data (inside the second domain) used in the simulations. The boundaries limit in the right image is the cities of MASP.

3. Results and Discussions

3.1. Surface Albedo

The albedo is an important surface property that influences directly in the intensity of UHI, since it acts in the primary heat storage source: It represents the ratio between reflected solar radiation by the surface and the incident solar radiation. Several studies show that the surface albedo change can reduce the UHI intensity, changing the type of constructed material, or even painting [21,74,75]. To evaluate this kind of purpose, two simulations were done comparing with the control simulation, changing only the building roof albedo. In the first simulation, the albedo was modified to 0.08, reducing in 55% of its original value. This value corresponds to asphalt. The second simulation tries to represent the cool roof condition, changing the surface albedo to 0.90, like a white painting roof.

Figure 4 shows the diurnal evolution of the UHI intensity in a central point of the MASP, comparing to the control simulation (with roof albedo equal to 0.18). The reduction of the roof albedo increases the UHI intensity to 0.2 °C. The negative peaks at 12 Z for both days correspond to the passage of the direct solar radiation from wall to roof, at 9:00 AM Local Time. This peak happens in all simulations. In the case of cool roof, the intensity of all urban areas decreases by 1 °C (Figure 5), at 15 Z. With more solar radiation being reflected by the roof surface, less radiation is absorbed, decreasing the temperature and the UHI intensity.

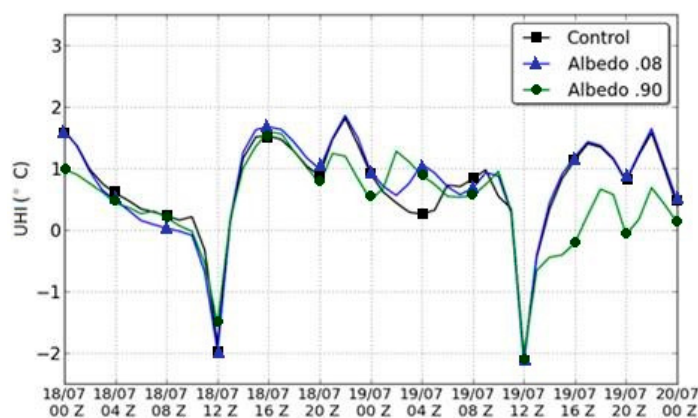


Figure 4. Diurnal evolution of Urban Heat Island (UHI) intensity for a central point of MASP. The black line represents the control simulation, the blue line the simulation with albedo equal to 0.08, and the green line the simulation with albedo equal to 0.90. Local Time equals Z-3 h.

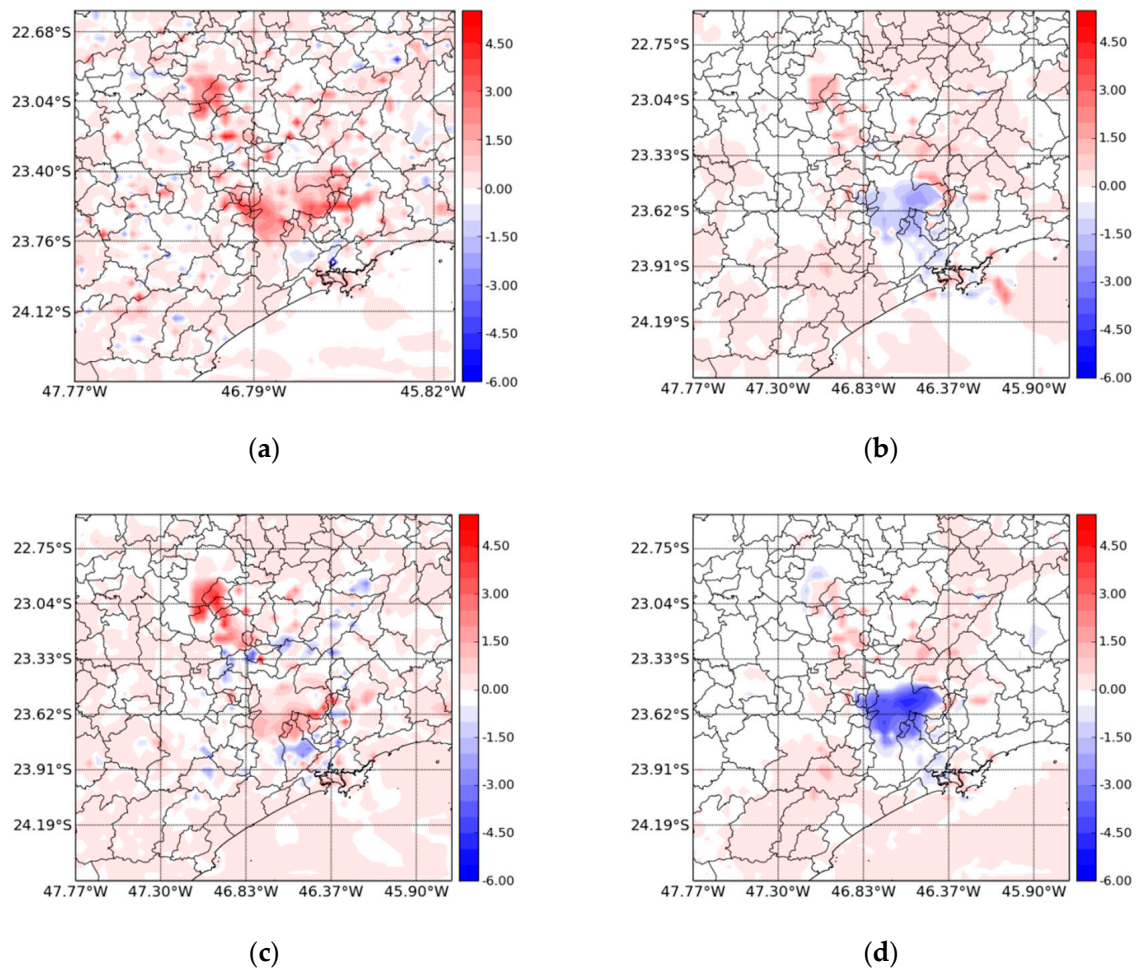


Figure 5. UHI intensity fields for 15 Z. Left column corresponds to the simulation with albedo equal to 0.08, and the right column, to the simulation equal to 0.90; (a,b) are for day 18, (c,d) for day 19.

3.2. Surface Emissivity

The emissivity has a fundamental role in the quantity of longwave radiation emitted by a surface. Its high value tends to reduce the temperature intensity during the day [76–78], because this surface emits thermal radiation.

In the control simulation, the wall, street and roof surfaces emissivity are 0.85, 0.90 and 0.90, respectively [37]. These values were set to 1, considering this a black body. This means that all absorbed radiation by each surface is re-emitted. Figure 6 shows the diurnal evolution of UHI intensity between the control simulation and the simulation setting up the emissivity value to 1. The results show that most of the night in both days, the UHI intensity has fewer values with higher emissivity. The difference between simulations is between 0.4 °C and 0.6 °C. These results are similar to the energy budget model developed by Oke et al. [79]. The maps in Figure 7 shows that the UHI intensity differences between both simulations can present a decrease in the adjacent rural region at 00Z of 19 July (blue colors in Figure 7b). With the same model, and for the same period, Morais et al. [53] showed that these differences in temperature are related to wind advection, which can transport heat from rural to urban regions. Therefore, the usage of a material similar to a black body can improve this heat transport.

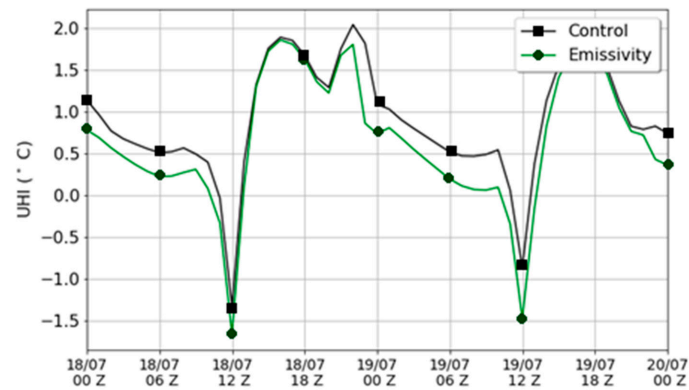


Figure 6. Diurnal evolution of UHI intensity for a central point of MASP. The black line represents the control simulation and green line, the simulation with emissivity increased to 1. Local Time equals Z–3 h.

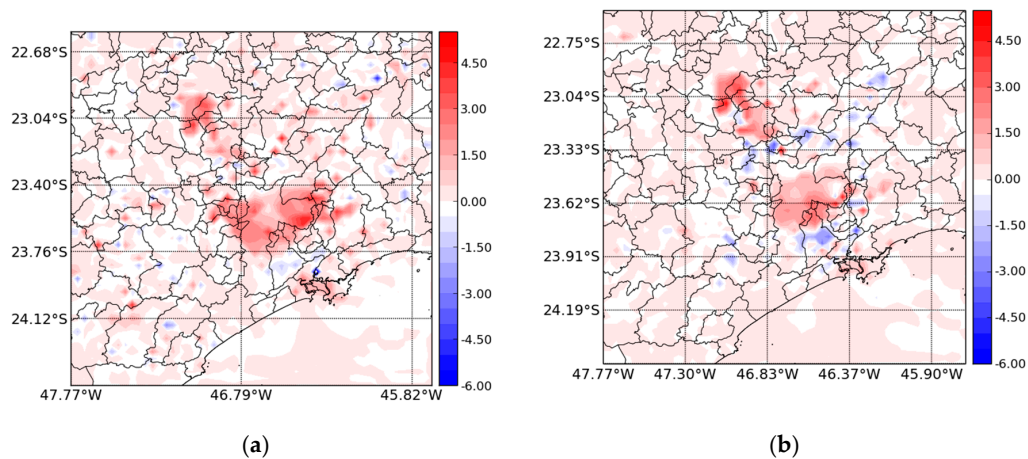


Figure 7. UHI intensity differences fields between all surface's emissivity equal to 1 simulation and control. (a) corresponds to 00Z for 18 July and (b) 00Z for 19 July.

3.3. Thermal Conductivity

The thermal conductivity has an impact on the material's temperature and, consequently, in the surface-air interface. Since conductivity shows how heat diffuses in a material, the reduction of its value should reduce the surface temperature, considering that the internal building temperature is constant.

Figure 8 shows the evolution of UHI intensity when thermal conductivity is reduced 10 times of its control simulation's value (Table 3), at a central point of MASP. In general, there is a reduction of its value, reaching 2 °C at 21 Z of 18 July. Hamdi and Schayes [80] attribute this reduction of air temperature inside the urban canyon to the wall effects, since it is the surface that receives direct solar radiation for a more extended period. In the case of the authors, the temperature differences were 3 °C in the sunset period, for Basel, Switzerland.

Table 3. Thermal conductivity values (in $\text{W}\cdot\text{m}^{-1}\cdot\text{K}^{-1}$) of control simulation for the three layers of each building surface in TEB. The values are similar to Freitas et al. [37]. For the sensitivity test, the thermal conductivity was reduced 10 times its original's values.

Surface	Layer 1	Layer 2	Layer 3
Wall	0.8100	0.8100	0.8100
Street	0.0103	1.0103	1.0103
Roof	0.4100	0.0500	0.0300

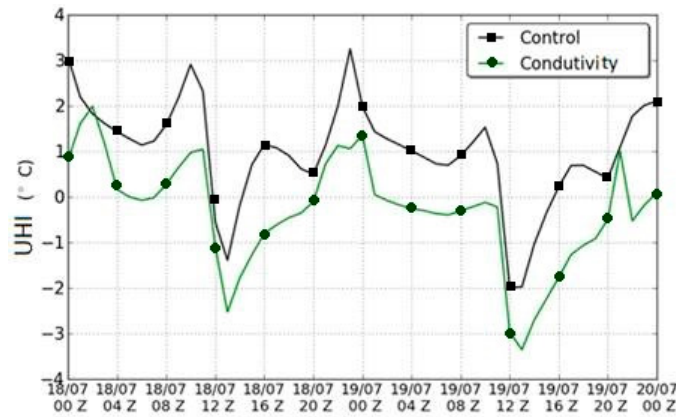


Figure 8. Diurnal evolution of UHI intensity for a central point of MASP. The black line represents the control simulation and green line, the simulation with thermal conductivity reduced 10 times. Local Time equals Z-3 h.

Analyzing the differences of UHI fields (Figure 9) for 15 Z, the central region of the urban area has decreased the temperature less than the adjacent area. As the aspect-ratio of this area is more significant, configuring a location with narrower urban canyons, it can retain more radiation [53,81]. Because of this effect, the UHI intensity difference in the central area of MASP is lower than the adjacent region.

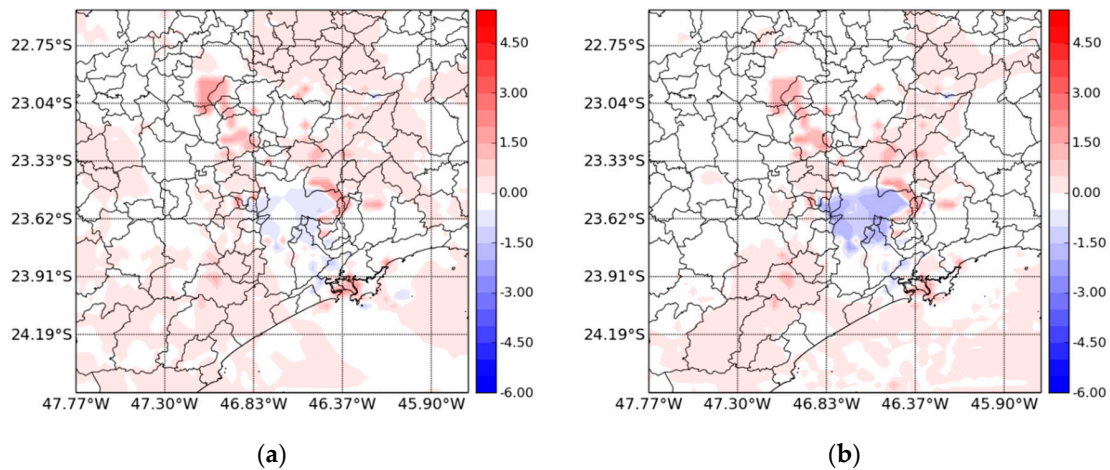


Figure 9. UHI intensity differences fields between simulation with reduction of thermal conductivity and control simulations; (a) corresponds to 15Z for 18 July and (b) 15Z for 19 July.

3.4. Heat Capacity

Like the thermal conductivity case, the change of heat capacity of material has an impact on the surface temperature and, consequently, in the surface-air interface. Figure 10 shows the evolution of UHI intensity for a central point of MASP with heat capacity increased in 10 times and its value for control simulation (Table 4). Similar to the reduction of thermal conductivity, the increase of heat capacity reduces the UHI intensity, with 3.5 °C at 00Z of 18 July. Also, the evolution shows that the beginning of the difference starts around 12 Z, when solar radiation reaches the street, indicating that this surface has an essential role in heat transferring in the urban atmosphere.

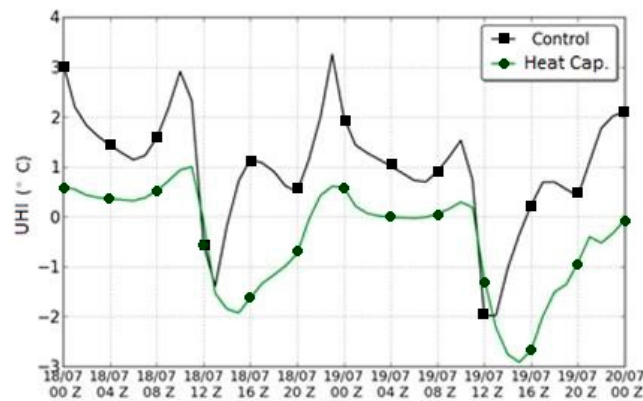


Figure 10. Diurnal evolution of UHI intensity for a central point of MASP. The black line represents the control simulation and green line, the simulation with heat capacity increased 10 times. Local Time equals Z–3 h.

Table 4. Heat capacity values (in $10^6 \text{ J}\cdot\text{K}\cdot\text{m}^{-3}$) of control simulation for the three layers of each building surface in TEB. The values are similar to Freitas et al. [37]. For the sensitivity test, the heat capacity was increased 10 times its original's values.

Surface	Layer 1	Layer 2	Layer 3
Wall	1.00	1.00	1.00
Street	1.24	1.28	1.28
Roof	2.11	0.28	0.29

The UHI intensity difference field (Figure 11) shows that the increase of the heat capacity reducing its value for all urban areas, with $2.4 \text{ }^\circ\text{C}$ at 15 Z of 19 July. The aspect-ratio also influences the temperature magnitude, since it can retain more radiation when taller buildings, or narrow streets, are presented [82,83].

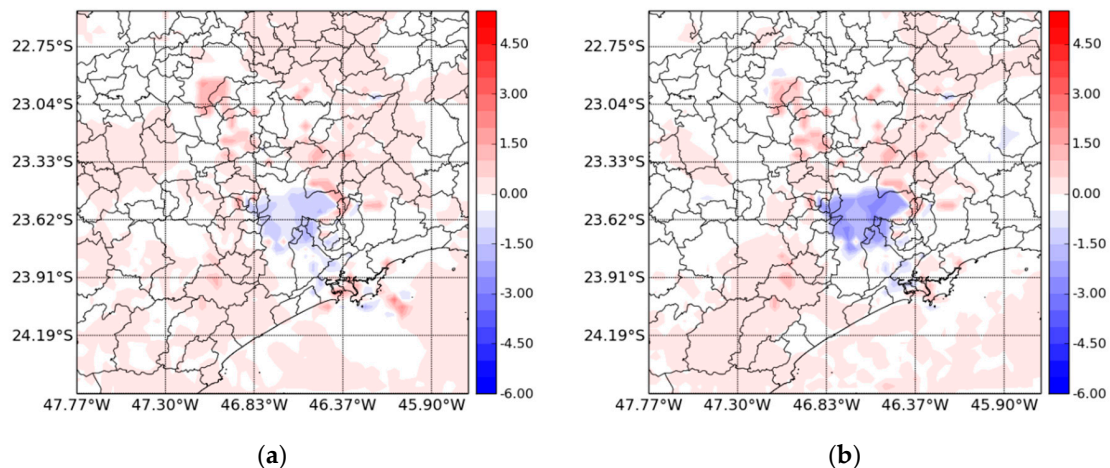


Figure 11. UHI intensity differences fields between simulation with heat capacity increased in 10 times and control simulations; (a) corresponds to 15Z for 18 July and (b) 15Z for 19 July.

Table 5 summarizes the results obtained in all experiments, considering the maximum reduction value of UHI intensity by both urban types and different experiments done. Only when roof surface albedo is 0.08, near to asphalt value, the temperature increases compared to control simulation. The changing of the other variables following this study criteria mean a decrease of UHI intensity.

Table 5. Summarizing the maximum UHI intensity reduction (in °C) by different urban-types and experiments with the control simulation. α is the surface albedo, ϵ is the surface emissivity, λ is the thermal conductivity and C, is the heat capacity.

	$\alpha = 0.9$	$\alpha = 0.08$	$\epsilon = 1$	λ (W·m ⁻¹ ·K ⁻¹)/10	C (J·m ⁻³ ·K ⁻¹) · 10
Urban-Type 1	2.50	−0.18	1.40	0.24	1.00
Urban-Type 2	1.20	−0.15	1.00	0.50	0.75

4. Conclusions and Remarks

Through atmospheric mesoscale modeling, the role of the physical properties of building materials in the urban thermal field of MASP was analyzed. The results obtained allow us to recognize the behavior of UHI's daily evolution, as well as the role of each parameter in the local climate. The radiative properties have a relevant impact when considering the effect of “cool roof”, increasing the value of albedo and blackbody, emitting more heat to the atmosphere and lowering the temperature of the entire urban surface. The solar radiation can be considered the main component in the energy budget, and the capacity of building material to reflect it in the roof contributes to a decrease in the temperature and the UHI intensity. A similar effect is observed for thermal properties, analyzing the heat capacity and thermal conductivity of the material. Even considering a simple urban canyon structure, these two properties play a key role in the turbulent flows in the urban boundary layer. The development of new materials seeking to vary the magnitudes of these properties as described in this study may contribute to the reduction of UHI intensity up to 3 °C for MASP. Among the materials that can contribute to this effect are cool pavements [84], green infrastructure [85], glass bead retro-reflective materials [86], concrete roads (with different radiative properties compared to asphalt) [87], and the use of Phase Change Materials (PCM) [88] on roofs. In summary, the increase of surface albedo, surface emissivity, thermal capacity and the reduction of thermal conductivity contributes to the reduction of UHI intensity by analyzing the different urban types in MASP.

It is important to highlight the role of building structure and orientation in the daily evolution of UHI, varying the radiative and thermal properties. In addition to the types of materials, future studies should consider that these variables must be taken into account in urban planning, seeking the minimum environmental impact caused by the urbanization process. Another important concept to study is the use of green infrastructures, such as green roofs and facades, and their interaction with these building material parameters. In this way, the use of mesoscale atmospheric models can be a useful tool in urban planning in an attempt to minimize the effects of urbanization on the local climate.

Author Contributions: Conceptualization, M.V.B.d.M., V.V.U.G., and E.D.d.F.; methodology, M.V.B.d.M., V.V.U.G., and E.D.d.F.; software, M.V.B.d.M. and E.D.d.F.; supervision, E.D.d.F.; validation, M.V.B.d.M., E.D.d.F. and E.R.M.; writing—original draft preparation, M.V.B.d.M., V.V.U.G., H.V. and I.V.-P.; writing—review & editing, M.V.B.d.M., H.V., C.C., R.A. and I.V.-P.

Funding: This research was funded by Fundação de Amparo a Pesquisa do Estado de São Paulo (FAPESP, grants 2011/01345-6, 2011/01040-0, and 2008/58104-8), the Conselho Nacional de Desenvolvimento Científico e Tecnológico (CNPq, grants 308963/2013-0 and 483354/2013-9), the Coordenação de Aperfeiçoamento de Pessoal de Nível Superior (CAPES), and the Universidad Catolica del Maule for the APC funding.

Acknowledgments: The authors would like to acknowledge Valery Masson (Centre National de Rescherches Météorologiques) and METEO-FRANCE for the use of the Town-Energy Budget.

Conflicts of Interest: The authors declare no conflict of interest.

References

1. United Nations. *World Urbanization Prospects: The 2018 Revision*; United Nations: New York, NY, USA, 2019.
2. Kalnay, E.; Cai, M. Impact of urbanization and land-use change on climate. *Nature* **2003**, *423*, 528–532. [[CrossRef](#)]
3. Oke, T.R. *Boundary Layer Climates*, 2nd ed.; Routledge: London, UK, 1987; ISBN 9780203407219.

4. Pielke, R.A.; Segal, M. Mesoscale Circulations Forced by Differential Terrain Heating. In *Mesoscale Meteorology and Forecasting*; Ray, P.S., Ed.; American Meteorological Society: Boston, MA, USA, 1986; pp. 516–548.
5. Rizwan, A.M.; Dennis, L.Y.C.; Liu, C. A review on the generation, determination and mitigation of Urban Heat Island. *J. Environ. Sci.* **2008**, *20*, 120–128. [[CrossRef](#)]
6. Oke, T.R. The energetic basis of the urban heat island. *Q. J. R. Meteorol. Soc.* **1982**, *108*, 1–24. [[CrossRef](#)]
7. Chen, F.; Kusaka, H.; Bornstain, R.; Ching, J.; Grimmond, C.S.B.; Grossman-Clarke, S.; Loridan, T.; Manning, K.; Martilli, A.; Miao, S.; et al. The integrated WRF/urban modeling system: Development, evaluation, and applications to urban environmental problems. *Int. J. Climatol.* **2011**, *31*, 273–288. [[CrossRef](#)]
8. García-Cueto, O.R.; Jáuregui-Ostos, E.; Toudert, D.; Tejada-Martinez, A. Detection of the urban heat island in Mexicali, B.C., México and its relationship with land use. *Atmósfera* **2007**, *20*, 111–131.
9. Ichinose, T.; Shimodozono, K.; Hanaki, K. Impact of anthropogenic heat on urban climate in Tokyo. *Atmos. Environ.* **1999**, *33*, 3897–3909. [[CrossRef](#)]
10. Mirzaei, P.A.; Haghighat, F. Approaches to study Urban Heat Island—Abilities and limitations. *Build. Environ.* **2010**, *45*, 2192–2201. [[CrossRef](#)]
11. Scalenghe, R.; Marsan, F.A. The anthropogenic sealing of soils in urban areas. *Landsc. Urban Plan.* **2009**, *90*, 1–10. [[CrossRef](#)]
12. Peng, B.; Williams, S.; Loughnan, M.; Lloyd, G.; Hansen, A.; Kjellstrom, T.; Dear, K.; Saniotis, A. The Effects of Extreme Heat on Human Mortality and Morbidity in Australia: Implications for Public Health. *Asia Pac. J. Public Health* **2011**, *23*, 27S–36S. [[CrossRef](#)]
13. Freitas, E.D.; Rozoff, C.M.; Cotton, W.R.; Dias, P.L.S. Interactions of an urban heat island and sea-breeze circulations during winter over the metropolitan area of São Paulo, Brazil. *Bound. Layer Meteorol.* **2007**, *122*, 43–65. [[CrossRef](#)]
14. Pellegatti Franco, D.M.; Andrade, M.F.; Ynoue, R.Y.; Ching, J. Effect of Local Climate Zone (LCZ) classification on ozone chemical transport model simulations in Sao Paulo, Brazil. *Urban Clim.* **2019**, *27*, 293–313. [[CrossRef](#)]
15. Yoshikado, H. Numerical Study of the Daytime Urban Effect and Its Interaction with the Sea Breeze. *J. Appl. Meteorol.* **1992**, *31*, 1146–1164.
16. Yoshikado, H. Interaction of the Sea Breeze with Urban Heat Islands of Different Sizes and Locations. *J. Meteorol. Soc. Jpn. Ser. II* **1994**, *72*, 139–143. [[CrossRef](#)]
17. Chen, T.; Sun, A.; Niu, R.; Chen, T.; Sun, A.; Niu, R. Effect of Land Cover Fractions on Changes in Surface Urban Heat Islands Using Landsat Time-Series Images. *Int. J. Environ. Res. Public Health* **2019**, *16*, 971. [[CrossRef](#)] [[PubMed](#)]
18. Morais, M.V.B.; Marciotto, E.R.; Urbina Guerrero, V.V.; Freitas, E.D. Effective albedo estimates for the Metropolitan Area of São Paulo using empirical sky-view factors. *Urban Clim.* **2017**, *21*, 183–194. [[CrossRef](#)]
19. Naserikia, M.; Asadi Shamsabadi, E.; Rafieian, M.; Leal Filho, W.; Naserikia, M.; Asadi Shamsabadi, E.; Rafieian, M.; Leal Filho, W. The Urban Heat Island in an Urban Context: A Case Study of Mashhad, Iran. *Int. J. Environ. Res. Public Health* **2019**, *16*, 313. [[CrossRef](#)] [[PubMed](#)]
20. Peña, M.A. Relationships between remotely sensed surface parameters associated with the urban heat sink formation in Santiago, Chile. *Int. J. Remote Sens.* **2008**, *29*, 4385–4404. [[CrossRef](#)]
21. Taha, H. Urban climates and heat islands: Albedo, evapotranspiration, and anthropogenic heat. *Energy Build.* **1997**, *25*, 99–103. [[CrossRef](#)]
22. Atkinson, B.W. Numerical modelling of urban heat-island intensity. *Bound. Layer Meteorol.* **2003**, *109*, 285–310. [[CrossRef](#)]
23. Montávez, J.P.; Rodríguez, A.; Jiménez, J.I. A study of the Urban Heat Island of Granada. *Int. J. Climatol.* **2000**, *20*, 899–911. [[CrossRef](#)]
24. Bowler, D.E.; Buyung-Ali, L.; Knight, T.M.; Pullin, A.S. Urban greening to cool towns and cities: A systematic review of the empirical evidence. *Landsc. Urban Plan.* **2010**, *97*, 147–155. [[CrossRef](#)]
25. Santamouris, M. Cooling the cities—A review of reflective and green roof mitigation technologies to fight heat island and improve comfort in urban environments. *Sol. Energy* **2014**, *103*, 682–703. [[CrossRef](#)]
26. Morais, M.V.B.; Freitas, E.D.; Urbina Guerrero, V.V.; Martins, L.D. A modeling analysis of urban canopy parameterization representing the vegetation effects in the megacity of São Paulo. *Urban Clim.* **2016**, *17*, 102–115. [[CrossRef](#)]

27. Qi, J.-D.; He, B.-J.; Wang, M.; Zhu, J.; Fu, W.-C. Do grey infrastructures always elevate urban temperature? No, utilizing grey infrastructures to mitigate urban heat island effects. *Sustain. Cities Soc.* **2019**, *46*, 101392. [[CrossRef](#)]
28. Santamouris, M.; Synnefa, A.; Karlessi, T. Using advanced cool materials in the urban built environment to mitigate heat islands and improve thermal comfort conditions. *Sol. Energy* **2011**, *85*, 3085–3102. [[CrossRef](#)]
29. Akbari, H.; Pomerantz, M.; Taha, H. Cool surfaces and shade trees to reduce energy use and improve air quality in urban areas. *Sol. Energy* **2001**, *70*, 295–310. [[CrossRef](#)]
30. Moser, A.; Uhl, E.; Rötzer, T.; Biber, P.; Caldentey, J.; Pretzsch, H. Effects of climate trends and drought events on urban tree growth in Santiago de Chile. *Cien. Invest. Agr.* **2018**, *45*, 35–50. [[CrossRef](#)]
31. Gupta, N.; Mathew, A.; Khandelwal, S. Analysis of cooling effect of water bodies on land surface temperature in nearby region: A case study of Ahmedabad and Chandigarh cities in India. *Egypt J. Remote Sens. Space Sci.* **2019**, *22*, 81–93. [[CrossRef](#)]
32. Morris, C.J.G.; Simmonds, I. Associations between varying magnitudes of the urban heat island and the synoptic climatology in Melbourne, Australia. *Int. J. Climatol.* **2000**, *20*, 1931–1954. [[CrossRef](#)]
33. Sang, J.; Liu, H.; Liu, H.; Zhang, Z. Observational and numerical studies of wintertime urban boundary layer. *J. Wind Eng. Ind. Aerodyn.* **2000**, *87*, 243–258. [[CrossRef](#)]
34. Sharma, A.; Conry, P.; Fernando, H.J.S.; Hamlet, A.F.; Hellmann, J.J.; Chen, F. Green and cool roofs to mitigate urban heat island effects in the Chicago metropolitan area: Evaluation with a regional climate model. *Environ. Res. Lett.* **2016**, *11*, 064004. [[CrossRef](#)]
35. Sharma, A.; Woodruff, S.; Budhathoki, M.; Hamlet, A.F.; Chen, F.; Fernando, H.J.S. Role of green roofs in reducing heat stress in vulnerable urban communities—A multidisciplinary approach. *Environ. Res. Lett.* **2018**, *13*, 094011. [[CrossRef](#)]
36. Georgescu, M. Challenges Associated with Adaptation to Future Urban Expansion. *J. Clim.* **2015**, *28*, 2544–2563. [[CrossRef](#)]
37. Song, J.; Wang, Z.-H.; Wang, C. The Regional Impact of Urban Heat Mitigation Strategies on Planetary Boundary Layer Dynamics Over a Semiarid City. *J. Geophys. Res. Atmos.* **2018**, *123*, 6410–6422. [[CrossRef](#)]
38. Morais, M.V.B.; Guerrero, V.V.U.; Martins, L.D.; Martins, J.A.; Morais, M.V.B.; Guerrero, V.V.U.; Martins, L.D.; Martins, J.A. Dynamical Downscaling of Future Climate Change Scenarios in Urban Heat Island and Its Neighborhood in a Brazilian Subtropical Area. *Proceedings* **2017**, *1*, 106. [[CrossRef](#)]
39. Patz, J.A.; Campbell-Lendrum, D.; Holloway, T.; Foley, J.A. Impact of regional climate change on human health. *Nature* **2005**, *438*, 310–317. [[CrossRef](#)]
40. Lundgren Kownacki, K.; Gao, C.; Kuklane, K.; Wierzbicka, A.; Lundgren Kownacki, K.; Gao, C.; Kuklane, K.; Wierzbicka, A. Heat Stress in Indoor Environments of Scandinavian Urban Areas: A Literature Review. *Int. J. Environ. Res. Public Health* **2019**, *16*, 560. [[CrossRef](#)]
41. Araujo, R.V.; Albertini, M.R.; Costa-da-Silva, A.L.; Suesdek, L.; Franceschi, N.C.S.; Bastos, N.M.; Katz, G.; Cardoso, V.A.; Castro, B.C.; Capurro, M.L.; et al. São Paulo urban heat islands have a higher incidence of dengue than other urban areas. *Braz. J. Infect. Dis.* **2015**, *19*, 146–155. [[CrossRef](#)]
42. Mironova, V.; Shartova, N.; Beljaev, A.; Varentsov, M.; Grishchenko, M.; Mironova, V.; Shartova, N.; Beljaev, A.; Varentsov, M.; Grishchenko, M. Effects of Climate Change and Heterogeneity of Local Climates on the Development of Malaria Parasite (*Plasmodium vivax*) in Moscow Megacity Region. *Int. J. Environ. Res. Public Health* **2019**, *16*, 694. [[CrossRef](#)]
43. Valdés, H.; Correa, C.; Mellado, F. Proposed model of sustainable construction skills for engineers in Chile. *Sustainability* **2018**, *10*, 3039. [[CrossRef](#)]
44. Brown, M.A.; Southworth, F. Mitigating Climate Change through Green Buildings and Smart Growth. *Environ. Plan. A* **2008**, *40*, 653–675. [[CrossRef](#)]
45. Letelier, V.; Ortega, J.; Tarela, E.; Muñoz, P.; Henríquez-Jara, B.; Moriconi, G. Mechanical Performance of Eco-Friendly Concretes with Volcanic Powder and Recycled Concrete Aggregates. *Sustainability* **2018**, *10*, 3036. [[CrossRef](#)]
46. Muñoz, P.; Mendivil, M.A.; Letelier, V.; Morales, M.P. Thermal and mechanical properties of fired clay bricks made by using grapevine shoots as pore forming agent. Influence of particle size and percentage of replacement. *Constr. Build. Mater.* **2019**, *224*, 639–658. [[CrossRef](#)]
47. Letelier, V.; Henríquez-Jara, B.I.; Manosalva, M.; Parodi, C.; Ortega, J.M. Use of Waste Glass as A Replacement for Raw Materials in Mortars with a Lower Environmental Impact. *Energies* **2019**, *12*, 1974. [[CrossRef](#)]

48. Ortega, J.M.; Letelier, V.; Solas, C.; Moriconi, G.; Climent, M.Á.; Sánchez, I. Long-term effects of waste brick powder addition in the microstructure and service properties of mortars. *Constr. Build. Mater.* **2018**, *182*, 691–702. [[CrossRef](#)]
49. Martilli, A.; Krayenhoff, E.S.; Nazarian, N. Is the Urban Heat Island intensity relevant for heat mitigation studies? *Urban Clim.* **2020**, *31*, 100541. [[CrossRef](#)]
50. IBGE Censo Demográfico. Available online: <https://www.ibge.gov.br/estatisticas/sociais/saude/9662-censo-demografico-2010.html?=&t=sobre> (accessed on 12 September 2019).
51. Duarte, D.H.S.; Shinzato, P.; Gusson, C.S.; Alves, C.A. The impact of vegetation on urban microclimate to counterbalance built density in a subtropical changing climate. *Urban Clim.* **2015**, *14*, 224–239. [[CrossRef](#)]
52. de Lima, G.N.; Magaña Rueda, V.O. The urban growth of the metropolitan area of Sao Paulo and its impact on the climate. *Weather Clim. Extrem.* **2018**, *21*, 17–26. [[CrossRef](#)]
53. Morais, M.V.B.; Freitas, E.D.; Marciotto, E.R.; Urbina Guerrero, V.V.; Martins, L.D.; Martins, J.A. Implementation of observed sky-view factor in a mesoscale model for sensitivity studies of the urban meteorology. *Sustainability* **2018**, *10*, 2183. [[CrossRef](#)]
54. Johansson, E.; Spangenberg, J.; Gouvêa, M.L.; Freitas, E.D. Scale-integrated atmospheric simulations to assess thermal comfort in different urban tissues in the warm humid summer of São Paulo, Brazil. *Urban Clim.* **2013**, *6*, 24–43. [[CrossRef](#)]
55. Stewart, I.D.; Oke, T.R.; Stewart, I.D.; Oke, T.R. Local Climate Zones for Urban Temperature Studies. *Bull. Am. Meteorol. Soc.* **2012**, *93*, 1879–1900. [[CrossRef](#)]
56. Freitas, S.R.; Panetta, J.; Longo, K.M.; Rodrigues, L.F.; Moreira, D.S.; Rosário, N.E.; Silva Dias, P.L.; Silva Dias, M.A.F.; Souza, E.P.; Freitas, E.D.; et al. The Brazilian developments on the Regional Atmospheric Modeling System (BRAMS 5.2): An integrated environmental model tuned for tropical areas. *Geosci. Model Dev.* **2017**, *10*, 189–222. [[CrossRef](#)]
57. Freitas, S.R.; Longo, K.M.; Silva Dias, M.A.F.; Chatfield, R.; Silva Dias, P.; Artaxo, P.; Andreae, M.O.; Grell, G.; Rodrigues, L.F.; Fazenda, A.; et al. The Coupled Aerosol and Tracer Transport model to the Brazilian developments on the Regional Atmospheric Modeling System (CATT-BRAMS)—Part 1: Model description and evaluation. *Atmos. Chem. Phys.* **2009**, *9*, 2843–2861. [[CrossRef](#)]
58. Cotton, W.R.; Pielke, R.A., Sr.; Walko, R.L.; Liston, G.E.; Tremback, C.J.; Jiang, H.; McAnelly, R.L.; Harrington, J.Y.; Nicholls, M.E.; Carrio, G.G.; et al. RAMS 2001: Current status and future directions. *Meteorol. Atmos. Phys.* **2003**, *82*, 5–29. [[CrossRef](#)]
59. Walko, R.L.; Band, L.E.; Baron, J.; Kittel, T.G.F.; Lammers, R.; Lee, T.J.; Ojima, D.; Pielke, R.A.; Taylor, C.; Tague, C.; et al. Coupled Atmosphere–Biophysics–Hydrology Models for Environmental Modeling. *J. Appl. Meteorol.* **2000**, *39*, 931–944. [[CrossRef](#)]
60. Masson, V. A physically-based scheme for the urban energy budget in atmospheric models. *Bound. Layer Meteorol.* **2000**, *94*, 357–397. [[CrossRef](#)]
61. Masson, V.; Grimmond, C.S.B.; Oke, T.R. Evaluation of the Town Energy Balance (TEB) Scheme with Direct Measurements from Dry Districts in Two Cities. *Am. Meteorol. Soc.* **2002**, *41*, 1011–1026.
62. Freitas, E.D.; Martins, L.D.; Silva Dias, P.L.; Andrade, M.F. A simple photochemical module implemented in RAMS for tropospheric ozone concentration forecast in the metropolitan area of São Paulo, Brazil: Coupling and validation. *Atmos. Environ.* **2005**, *39*, 6352–6361. [[CrossRef](#)]
63. McMullan, R. *Environmental Science in Building*; Macmillan Education: London, UK, 1998; ISBN 978-0-333-73201-4.
64. Martilli, A.; Clappier, A.; Rotach, M.W. An Urban Surface Exchange Parameterisation for Mesoscale Models. *Bound. Layer Meteorol.* **2002**, *104*, 261–304. [[CrossRef](#)]
65. Johnson, G.T.; Oke, T.R.; Lyons, T.J.; Steyn, D.G.; Watson, I.D.; Voogt, J.A. Simulation of surface urban heat islands under ‘IDEAL’ conditions at night part 1: Theory and tests against field data. *Bound. Layer Meteorol.* **1991**, *56*, 275–294. [[CrossRef](#)]
66. NBR15220 Desempenho Térmico de Edificações Parte 1: Definições, Símbolos e Unidades 2003, 66. Available online: <https://www.abntcatalogo.com.br/norma.aspx?ID=635> (accessed on 2 December 2019).
67. Klemp, J.B.; Wilhelmson, R.B.; Klemp, J.B.; Wilhelmson, R.B. The Simulation of Three-Dimensional Convective Storm Dynamics. *J. Atmos. Sci.* **1978**, *35*, 1070–1096. [[CrossRef](#)]
68. Chen, C.; Cotton, W.R. A one-dimensional simulation of the stratocumulus-capped mixed layer. *Bound. Layer Meteorol.* **1983**, *25*, 289–321. [[CrossRef](#)]

69. Smagorinsky, J. General Circulation Experiments with the primitive equations. *Mon. Weather Rev.* **1963**, *91*, 99–164. [CrossRef]
70. Hill, G.E. Factors Controlling the Size and Spacing of Cumulus Clouds as Revealed by Numerical Experiments. *J. Atmos. Sci.* **1974**, *31*, 646–673. [CrossRef]
71. Lilly, D.K. On the numerical simulation of buoyant convection. *Tellus* **1962**, *14*, 148–172. [CrossRef]
72. Daley, R. *Atmospheric Data Analysis*; Cambridge University Press: Cambridge, UK, 1991.
73. Didan, K. MOD13Q1 MODIS/Terra Vegetation Indices 16-Day L3 Global 250m SIN Grid V006 [Data set]. Available online: <https://doi.org/10.5067/MODIS/MOD13Q1.006> (accessed on 5 October 2019).
74. Li, D.; Bou-Zeid, E.; Oppenheimer, M. The effectiveness of cool and green roofs as urban heat island mitigation strategies. *Environ. Res. Lett.* **2014**, *9*, 055002. [CrossRef]
75. Oleson, K.W.; Bonan, G.B.; Feddema, J. Effects of white roofs on urban temperature in a global climate model. *Geophys. Res. Lett.* **2010**, *37*, L03701. [CrossRef]
76. Family, R.; Mengüç, M. Analysis of Sustainable Materials for Radiative Cooling Potential of Building Surfaces. *Sustainability* **2018**, *10*, 3049. [CrossRef]
77. Hoshyar, H.A.; Rahimipetroudi, I.; Ganji, D.D. Heat Transfer Performance on Longitudinal Porous Fins with Temperature-Dependent Heat Generation, Heat Transfer Coefficient and Surface Emissivity. *Iran. J. Sci. Technol. Trans. Mech. Eng.* **2019**, *43*, 383–391. [CrossRef]
78. Ferreira, M.J.; de Oliveira, A.P.; Soares, J.; Codato, G.; Bárbaro, E.W.; Escobedo, J.F. Radiation balance at the surface in the city of São Paulo, Brazil: Diurnal and seasonal variations. *Theor. Appl. Climatol.* **2012**, *107*, 229–246. [CrossRef]
79. Oke, T.R.; Johnson, G.T.; Steyn, D.G.; Watson, I.D. Simulation of surface urban heat islands under ‘ideal’ conditions at night part 2: Diagnosis of causation. *Bound. Layer Meteorol.* **1991**, *56*, 339–358. [CrossRef]
80. Hamdi, R.; Schayes, G. Sensitivity study of the urban heat island intensity to urban characteristics. *Int. J. Climatol.* **2008**, *28*, 973–982. [CrossRef]
81. Marciotto, E.R. Variability of energy fluxes in relation to the net-radiation of urban and suburban areas: A case study. *Meteorol. Atmos. Phys.* **2013**, *121*, 17–28. [CrossRef]
82. Aida, M.; Gotoh, K. Urban Albedo as a Function of The Urban Structure—A two-dimensional numerical Simulation. *Bound. Layer Meteorol.* **1982**, *23*, 415–424. [CrossRef]
83. Fortuniak, K. Numerical estimation of the effective albedo of an urban canyon. *Theor. Appl. Climatol.* **2007**, *91*, 245–258. [CrossRef]
84. Qin, Y. A review on the development of cool pavements to mitigate urban heat island effect. *Renew. Sustain. Energy Rev.* **2015**, *52*, 445–459. [CrossRef]
85. Aflaki, A.; Mirnezhad, M.; Ghaffarianhoseini, A.; Ghaffarianhoseini, A.; Omrany, H.; Wang, Z.-H.; Akbari, H. Urban heat island mitigation strategies: A state-of-the-art review on Kuala Lumpur, Singapore and Hong Kong. *Cities* **2017**, *62*, 131–145. [CrossRef]
86. Yuan, J.; Emura, K.; Sakai, H.; Farnham, C.; Lu, S. Optical analysis of glass bead retro-reflective materials for urban heat island mitigation. *Sol. Energy* **2016**, *132*, 203–213. [CrossRef]
87. Kakoniti, A.; Georgiou, G.; Marakkos, K.; Kumar, P.; Neophytou, M.K.-A. The role of materials selection in the urban heat island effect in dry mid-latitude climates. *Environ. Fluid Mech.* **2016**, *16*, 347–371. [CrossRef]
88. Chung, M.H.; Park, J.C. Development of PCM cool roof system to control urban heat island considering temperate climatic conditions. *Energy Build.* **2016**, *116*, 341–348. [CrossRef]

